applied sciences

MDPI

Article

Analysis of Elastoplastic Mechanical Properties of Non-Uniform Frozen Wall Considering Frost Heave

Bin Wang [1,2,3,*], Shenwei Liang [1], Yi Cao [1], Chuanxin Rong [1,3] and Shengmin Yu [1]

[1] School of Civil Engineering and Architecture, Anhui University of Science and Technology, Huainan 232001, China
[2] Postdoctoral Research Station, China Coal Mine Construction Group Co., Ltd., Hefei 230091, China
[3] Engineering Research Center of Underground Mine Construction, Ministry of Education, Anhui University of Science and Technology, Huainan 232001, China
* Correspondence: wangbin@aust.edu.cn; Tel.: +86-182-9760-9818

Abstract: The aim of this study was to analyze the force and deformation law of an artificial frozen wall. Thus, the frost heave coefficient was introduced to describe the frost heave characteristics, and the frozen wall was regarded as a heterogeneous material whose material properties changed in a parabolic pattern with the radius. The elastoplastic stress and displacement formulas of a non-uniform frozen wall considering frost heave characteristics were derived according to different strength criteria. Consequently, the derived formulas were used to calculate and analyze the mechanical characteristics of the artificial frozen wall. The results showed that the radial stress of the frozen wall changed linearly, whereas the circumferential stress change followed a parabolic pattern after considering the non-uniform characteristics. Moreover, the displacement of the outer edge of the frozen wall was always greater than that of the inner edge, and the displacement of the inner edge changed with the increasing temperature, significantly greater than that of the outer edge. When the frozen wall was in the elastic state, its displacement caused by frost heave was constant. When the frozen wall entered the elastic–plastic state, the displacement of its inner edge caused by frost heave increased with the increase in the radius of the plastic zone, whereas the displacement of the outer edge caused by frost heave decreased with the increase in the radius of the plastic zone.

Keywords: artificial ground freezing method; nonuniform frozen wall; frost heave; elastoplastic analysis; analytical solution

check for updates

Citation: Wang, B.; Liang, S.; Cao, Y.; Rong, C.; Yu, S. Analysis of Elastoplastic Mechanical Properties of Non-Uniform Frozen Wall Considering Frost Heave. *Appl. Sci.* **2023**, *13*, 1038. https://doi.org/10.3390/app13021038

Academic Editors: Jun Hu, Jie Zhou and Kai-Qi Li

Received: 12 December 2022
Revised: 10 January 2023
Accepted: 11 January 2023
Published: 12 January 2023

Copyright: © 2023 by the authors. Licensee MDPI, Basel, Switzerland. This article is an open access article distributed under the terms and conditions of the Creative Commons Attribution (CC BY) license (https://creativecommons.org/licenses/by/4.0/).

1. Introduction

The AGF (artificial ground freezing method) has been widely used in underground engineering construction in water-rich strata because the resultant frozen wall has a good isolation effect on the groundwater [1–4], the principle of AGF is shown in Figure 1. In the construction of shaft freezing method, the depth of the frozen wall depends on the buried depth of mineral resources. For example, the freezing depth of Polby potash salt mine in the UK reached 930 m, and the freezing depth of the auxiliary shaft of Hutaoyu coal mine in China's Gansu Province reached 950 m [5]. The frozen soil undergoes frost heaving during the formation freezing, which is caused by the migration of unfrozen water and the expansion of frozen soil. The deformation of stratum is the main cause of the damage of an underground building structure [6–8], and the frost heaving is a major cause of the fracture of freezing pipes and the deformation of surrounding strata of underground buildings [9,10].

Currently, research on frost heave of stratum has been mainly focused on two aspects: the frost heave of frozen surrounding rock of tunnels in cold areas and the frost heave caused by the freezing of artificial formations. In the theoretical calculation of the frost heave force of tunnels in cold regions, Zhang et al. [11–13] used the unified strength theory as the basis for determining tunnels, considering the comprehensive influence of the intermediate

principal stress and transverse isotropic frost heave on the strength of the surrounding rock. They established the unified plastic analytical solution of the stress and displacement of tunnels in cold areas. Xia et al. [14,15] found an analytical solution of the frost heave force of tunnels in cold areas. In this solution, the anisotropic frost heave coefficient k describes the transverse isotropic frost heave of the surrounding rock. The rationality of the solution was verified by comparing its results with field data. Feng [16] established a model for determining the elasticity and plasticity of the surrounding rock of tunnels in cold zones. Liu [17] divided the frozen surrounding rock into partitions according to support strength and support time, established a calculation model that considers the influence of frost heave, and examined the stress and deformation of tunnel lining and surrounding rock in cold areas through engineering cases. Zhang [18] established a three-dimensional temperature field model based on the test results of the temperature field of a tunnel in a cold region, obtaining the variation rule of the freezing depth of surrounding rock using Stephen's formula. In addition, the author established a new frost heave model based on the freezing depth of surrounding rock, combined with the frost heave model of a freeze–thaw zone and the frost heave model of regolith. Jiang et al. [19] established an elastic–plastic damage mechanics calculation model, considering the characteristics of the uneven frost heave of surrounding rock, verifying the theoretical solutions and analyzing the parameters.

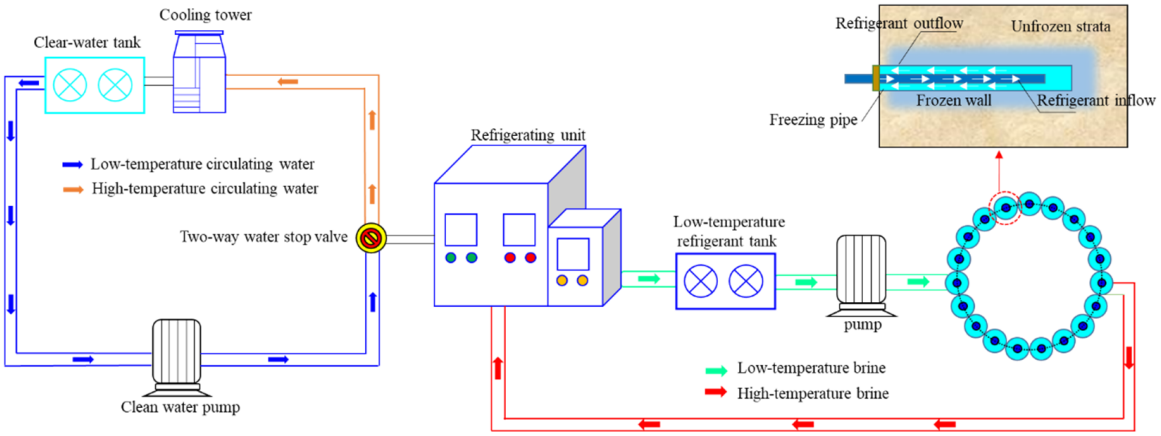


Figure 1. Schematic diagram of AGF.

Unlike the frozen surrounding rock of a tunnel in a cold zone, the artificial frozen wall is generated by freezing pipes. The heat conduction distance of freezing pipes and the direction of the temperature gradient influence the temperature within the frozen wall, which changes with the distance from the freezing pipes. Consequently, the internal strength of the frozen wall is non-uniform. The difference between the frozen surrounding rock of a tunnel and an artificial frozen wall is shown in Figure 2. If a frozen wall is treated as a homogeneous material to determine its mechanical properties, errors would be encountered in the calculation. Hu [20,21] derived a stress model for the frozen wall of single-row and double-row pipes using the M–C yield criterion. Wang et al. proposed a stress calculation formula for the heterogeneous frozen wall of three-row pipes [22] and derived a model for the directional-seepage-induced stress of the heterogeneous frozen wall by considering the influence of groundwater on the temperature distribution [23]. As a frozen wall does not exist in isolation in the soil, the unfrozen soil interacts with the frozen wall. Thus, soil excavation within the frozen wall influences the mechanical state of the wall. Yang et al. deduced the elastic–plastic stress solution of a frozen wall by considering the interaction of the wall with surrounding rock [24]. Wang developed a stress formula for the heterogeneous frozen wall, and the formula considers the unloading action and interaction with the unfrozen body [25].

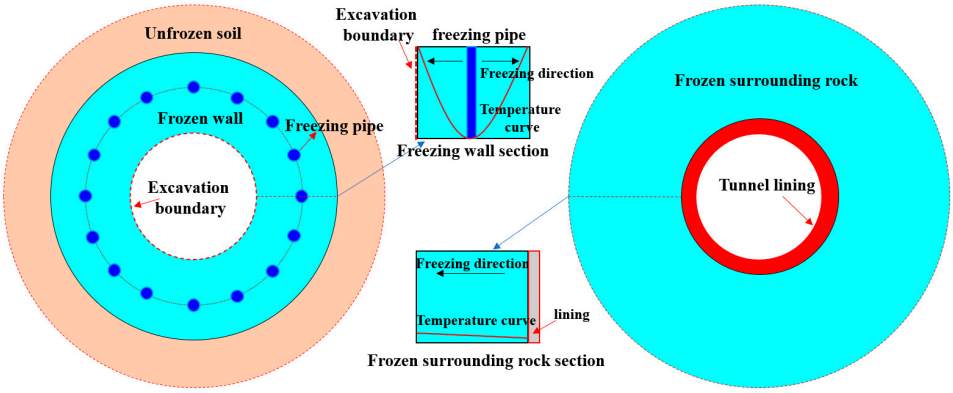


Figure 2. The difference between the frozen surrounding rock of a tunnel and an artificial frozen wall.

Currently, research on the theoretical calculation of the frost heave force of frozen surrounding rock of a tunnel in a cold area is relatively mature. Similarly, research on the mechanical mechanism of a heterogeneous frozen wall has advanced to appreciable levels. However, no relevant results have been obtained on the elastoplastic mechanical properties of a non-uniform frozen wall considering frost heave. The artificial frozen wall is different from frozen surrounding rock. The surrounding rock of a tunnel in a cold area is affected by unidirectional temperature gradient, which means it can be considered as a homogeneous material. However, the artificial frozen wall is formed using a freezing pipe; the temperature near the freezing pipe is low, whereas the temperature near the freezing front is high, resulting in the variation of the material properties of the frozen wall with the distance from the freezing pipe. In this case, the frost heave calculation theory of homogeneous frozen surrounding rock in a cold-region tunnel would not yield accurate calculation results of the stress and displacement of an artificial frozen wall. Therefore, the aim of this study is to introduce a frost heaving coefficient to describe the frost heaving characteristics of a frozen wall. The frozen wall is regarded as a functionally graded material whose material properties change parabolically with radius. The calculation formulas of the elastoplastic stress and displacement of a non-uniform frozen wall are derived using different strength criteria and considering frost heaving characteristics. This study is expected to provide a more accurate theoretical method for analyzing the mechanical properties of an artificial frozen wall.

2. Basic Assumptions and Frozen Soil Parameters

2.1. Basic Assumptions

1. Unfrozen soil is a homogeneous and an isotropic elastic medium [20–25]. The frozen wall is a heterogeneous material whose material properties vary with the wall radius [20–23];
2. The frost heave coefficient remains unchanged during freezing, and the frost heave rates of tangential and radial lines are unequal and remain unchanged during the freezing [14,15];
3. The Poisson's ratio μ and internal friction angle φ remain unchanged before and after freezing [20–23];
4. After entering the plastic state, the wall volume becomes incompressible [20–25];
5. The mechanical characteristics of the frozen wall are simplified as an axisymmetric plane strain problem [20–25].

2.2. Nonuniform Frost Heave Characteristics of Frozen Wall

An obvious temperature gradient exists between a freezing pipe and the surrounding soil during an artificial freezing process. The unfrozen water migrates to the freezing front along the temperature gradient, resulting in uneven frost heaving. The frost heave

deformation along the direction of the temperature gradient $\alpha_{\parallel}$ is greater than that of the vertical temperature gradient $\alpha_{\perp}$.

The inhomogeneous frost heave coefficient k of soil is defined as

$$k = \alpha_{\parallel} / \alpha_{\perp}. \tag{1}$$

$k > 1$ represents the nonuniform frost heave characteristics of the frozen wall. The frost heave rate of the radial line of the frozen wall $\alpha_r = \alpha_{\parallel}$, and the circumferential frost heave rate $\alpha_\theta = \alpha_{\perp}$. As the axis direction of the frozen wall is perpendicular to the direction of the frozen soil, the linear frost heave rate along the axis is approximately equal to the circumferential linear frost heave rate. Thus, the volume frost heave rate of the frozen soil can be expressed as follows [11,14]:

$$\alpha_v = \alpha_r + \alpha_z + \alpha_\theta = \alpha_r + 2\alpha_\theta. \tag{2}$$

The relationship between α_v and k, α_r, and α_θ satisfies the following equations [11,14]:

$$\alpha_r = \frac{k\alpha_v}{k+2}, \tag{3}$$

$$\alpha_\theta = \frac{\alpha_v}{k+2}. \tag{4}$$

2.3. Equivalent Temperature Field of Frozen Wall

A linear relationship exists between the material properties of frozen soil and temperature [20], and the quadratic function curve reflects the temperature of the middle section of the adjacent freezing pipe within the range of freezing temperature commonly used in engineering practice [20]. Therefore, the elastic modulus and cohesion can be expressed in the following form:

$$E(r) = ar^2 + br + c \quad r \in [r_1, r_2], \tag{5}$$

$$c(r) = mr^2 + nr + l \quad r \in [r_1, r_2], \tag{6}$$

where a, b, c and m, l, n are the parameters related to the temperature distribution curve.

2.4. Strength Criteria for Frozen Soil

The strength criterion of frozen soil can be uniformly expressed as [24]

$$\sigma_\theta = M\sigma_r + Bc. \tag{7}$$

The values of M and B are presented in Table 1.

Table 1. Expressions of M and B.

Strength Criteria	M	B
Mohr–Coulomb criteria	$\frac{1 + \sin\varphi}{1 - \sin\varphi}$	$-\frac{2\cos\varphi}{1 - \sin\varphi}$
Druker–Prager criteria	$\frac{1 + 3\alpha}{1 - 3\alpha}$	$-\frac{2\kappa}{1 - 3\alpha}$
Tresca criteria	$\frac{1 + 2\sqrt{3}\alpha}{1 - 2\sqrt{3}\alpha}$	$-\frac{4\sqrt{3}\kappa}{3\left(1 - 2\sqrt{3}\alpha\right)}$
Twin shear unified failure criterion	$\frac{2(1 + b)(1 + \sin\varphi) - (1 - \sin\varphi)b}{(1 - \sin\varphi)(b + 2)}$	$-\frac{2(1 + b)}{(b + 2)}\frac{2\cos\varphi}{1 - \sin\varphi}$

where $\alpha = \frac{\sin\varphi}{\sqrt{3}\sqrt{3 + \sin^2\varphi}}$ $\kappa = -\frac{\sqrt{3}\cos\varphi}{\sqrt{3 + \sin^2\varphi}}$.

3. Analytical Solution of Stress and Displacement of Frozen Wall

The research flowchart of this study is depicted in Figure 3.

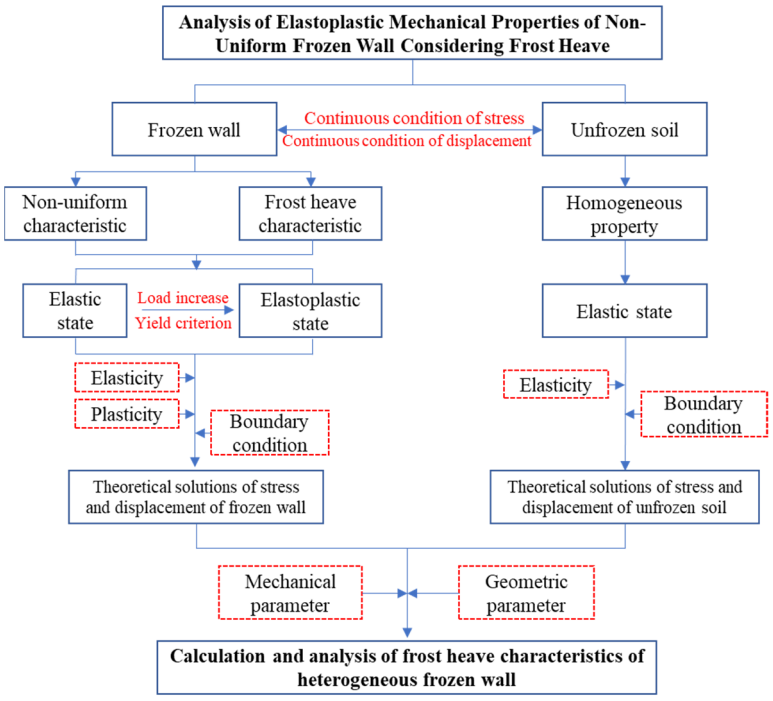


Figure 3. Research flowchart.

3.1. Mechanical Calculation Model of Frozen Wall

The mechanical model is depicted in Figure 4. In this model, P_0 is the formation pressure borne by the unfrozen body at infinity, P_1 is the external load exerted by the unfrozen body, and P_ρ is the interaction force at the junction of the plastic zone and the elastic zone. The inner and outer diameters of the frozen wall are denoted by R_1 and R_2, respectively, and the radius of any point on the section of the frozen wall is denoted by R. To facilitate the formula derivation, the relative radius $r = R/R_1$ is used to represent any point in the frozen wall section.

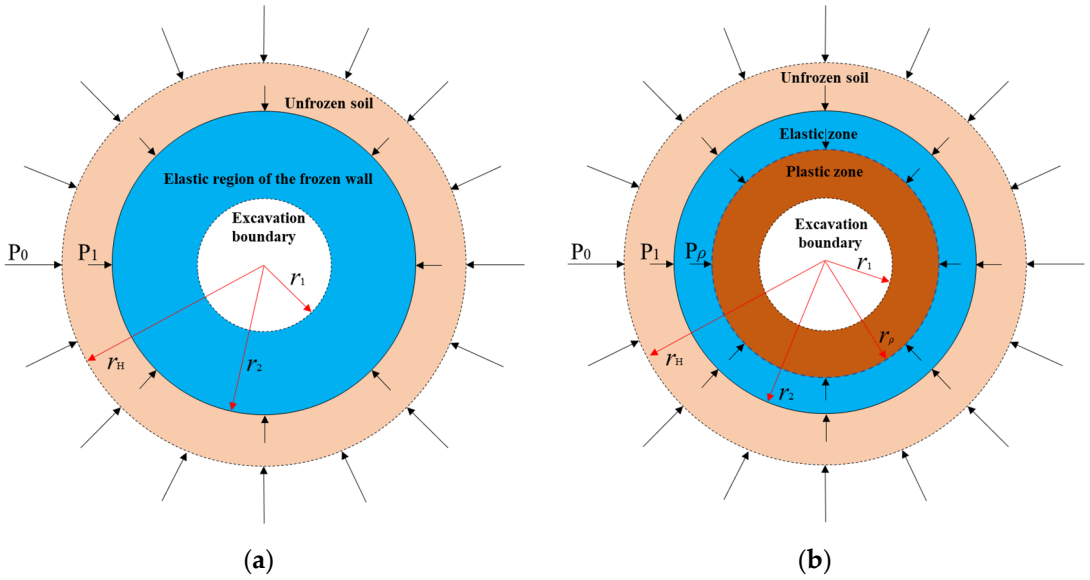


Figure 4. Mechanical calculation model of frozen wall. (**a**) Elastic model. (**b**) Elastoplastic model.

At the inner diameter: $R_1/R_1 = 1$
At the elastic–plastic boundary: $R_\rho/R_1 = r_\rho$
At the outer diameter: $R_2/R_1 = r_2$
At infinity: $R_\infty/R_1 = r_\infty$

When the external load is small, the frozen wall is in an elastic state. The mechanical model in this state is depicted in Figure 4a and comprises two parts: frozen wall $r \in [r_1, r_2]$ and unfrozen soil $r \in [r_2, r_\infty)$. When the external load is greater than its elastic ultimate bearing capacity, the frozen wall enters the elastoplastic state. The mechanical model in this state is depicted in Figure 4b. Here, the mechanical model mainly comprises three parts: plastic zone ($r \in [r_1, r_\rho]$), elastic zone ($r \in [r_\rho, r_2]$), and unfrozen soil ($r \in [r_2, r_\infty)$).

3.2. Calculation of Elastic Stress of Frozen Wall

When the frozen wall is in an elastic state, the calculation model shown in Figure 4a is used, and the boundary conditions of the model are as follows:

$$\begin{cases} \sigma_r^e = 0 \ \ (r = r_1) \\ \sigma_r^e = P_1 \ \ (r = r_2) \\ \sigma_r^s = P_0 \ \ (r = r_\infty) \\ U_r^e = U_r^s \ \ (r = r_2) \end{cases} \tag{8}$$

3.2.1. Unfrozen Area

The unfrozen soil is regarded as a uniform and elastic medium. Therefore, the formulas for calculating the elastic stress and displacement of the surrounding unfrozen soil are as follows [12,13]:

$$\sigma_r^s = \frac{r_2^2 r_\infty^2}{r_\infty^2 - r_2^2} \frac{P_1 - P_0}{r^2} + \frac{r_\infty^2 P_0 - r_2^2 P_1}{r_\infty^2 - r_2^2} = \left(1 - \frac{r_2^2}{r^2}\right) P_0 + \frac{r_2^2}{r^2} P_1 \tag{9}$$

$$\sigma_\theta^s = \frac{r_2^2 r_\infty^2}{r_\infty^2 - r_2^2} \frac{P_0 - P_1}{r^2} + \frac{r_\infty^2 P_0 - r_2^2 P_1}{r_\infty^2 - r_2^2} = \left(1 + \frac{r_2^2}{r^2}\right) P_0 - \frac{r_2^2}{r^2} P_1 \tag{10}$$

$$U^s = \frac{(1 + \mu_3)(P_0 - P_1) r_2^2}{E_3 r} \tag{11}$$

where E_3 and μ_3 are the elastic modulus and Poisson's ratio of unfrozen soil, respectively, and the superscript s represents the unfrozen zone. The field measurement results show that the material properties of frozen soil and the surrounding unfrozen soil are the same; to simplify the calculation, let $E_3 = E(r_2)$ and $\mu_3 = \mu_2$.

3.2.2. Frozen Wall

When the frozen wall was in the elastic plane strain state, the following basic equations are satisfied:

Equation of equilibrium [24]:

$$\frac{d\sigma_r}{dr} + \frac{\sigma_r - \sigma_\theta}{r} = 0 \tag{12}$$

Geometric equation [24]:

$$\begin{cases} \varepsilon_r = du_r/dr \\ \varepsilon_\theta = u_r/r \end{cases} \tag{13}$$

Considering the condition of non-uniform frost heaving, the physical equation under plane strain in the elastic region is:

$$\begin{cases} \varepsilon_r^e = \frac{1-\mu_2{}^2}{E(r)}\sigma_r - \frac{\mu_2(1+\mu_2)}{E(r)}\sigma_\theta + (\alpha_r + \mu_2\alpha_\theta) \\ \varepsilon_\theta^e = \frac{1-\mu_2{}^2}{E(r)}\sigma_\theta - \frac{\mu_2(1+\mu_2)}{E(r)}\sigma_r + (\alpha_\theta + \mu_2\alpha_r) \end{cases} \tag{14}$$

Introducing the stress function φ, σ_r and σ_θ are represented by φ:

$$\begin{cases} \sigma_r = \varphi/r \\ \sigma_\theta = \overset{\bullet}{\varphi} \end{cases} \tag{15}$$

Combining (12)–(15) yields the following formula:

$$r^2\varphi'' + r\left(1 - \frac{E'(r)}{E(r)}r\right)\varphi' + \left(\frac{E'(r)}{E(r)}r - 1\right)\varphi = \frac{r(\alpha_r - \alpha_\theta)E(r)}{1+\mu_2} \tag{16}$$

As mentioned in Section 2.3, the elastic modulus changes with the relative radius r, and the expression of the elastic modulus $E(r)$ is substituted into Equation (16) to obtain

$$r^2\varphi'' - r\frac{ar^2 - \mathrm{c}}{ar^2+br+c}\varphi' + \frac{ar^2-c}{ar^2+br+c}\varphi = \frac{(k-1)\alpha_v(ar^2+br+c)r}{(k+2)(1+\mu_2)} \tag{17}$$

Equation (17) is a second-order differential equation with variable coefficients, and the general solution is

$$\varphi = rC_0\left(a\ln r - b\frac{1}{r} - \frac{\mathrm{c}}{2}\frac{1}{r^2}\right) + B_0 r + rA_0(ar^2 + 2br + 2c\ln r - c) \tag{18}$$

where $A_0 = \frac{\alpha_v(k-1)}{4(k+2)(\mu_2+1)}$.

By substituting the boundary condition in Equation (8) into Equation (18), the following is obtained:

$$C_0 = \frac{-P_1 - A_0(a(r_1^2 - r_2^2) + 2b(r_1 - r_2) + 2c\ln(r_1/r_2))}{a\ln(r_1/r_2) + b\left(\frac{1}{r_2} - \frac{1}{r_1}\right) + \frac{c}{2}\left(\frac{1}{r_2^2} - \frac{1}{r_1^2}\right)} \tag{19}$$

$$B_0 = -A_0(ar_1^2 + 2br_1 + 2c\ln r_1 - c) - C_0\left(a\ln r_1 - b\frac{1}{r_1} - \frac{\mathrm{c}}{2}\frac{1}{r_1^2}\right) \tag{20}$$

$$\begin{cases} \sigma_r^e = \frac{A_0A_2(A_5-A_3)+(P_1+A_0A_1)(A_4-A_6)}{A_2} \\ \sigma_\theta^e = \frac{A_0A_2(A_8-A_3)+(P_1+A_0A_1)(A_4-A_7)}{A_2} \end{cases} \quad r \in [r_1, r_2] \tag{21}$$

where $A_1 = a(r_1^2 - r_2^2) + 2b(r_1 - r_2) + 2c\ln(r_1/r_2)$, $A_2 = a\ln(r_1/r_2) + b\left(\frac{1}{r_2} - \frac{1}{r_1}\right) + \frac{c}{2}\left(\frac{1}{r_2^2} - \frac{1}{r_1^2}\right)$, $A_3 = ar_1^2 + 2br_1 + 2c\ln r_1 - c$, $A_4 = a\ln r_1 - b\frac{1}{r_1} - \frac{c}{2}\frac{1}{r_1{}^2}$, $A_5 = ar^2 + 2br + 2c\ln r - c$, $A_6 = a\ln r - \frac{b}{r} - \frac{c}{2}\frac{1}{r^2}$, $A_7 = a\ln r + \frac{c}{2}\frac{1}{r^2} + a$, $A_8 = 3ar^2 + 4br + 2c\ln r + c$.

By substituting Equation (21) into physical Equation (14) and geometric Equation (13), the analytical solution of the elastic displacement of the heterogeneous frozen wall considering frost heave characteristics is obtained:

$$U^e = \frac{r\cdot(1-\mu_2^2)}{E(r)}\cdot\sigma_\theta^e - \frac{r\cdot\mu_2(1+\mu_2)}{E(r)}\cdot\sigma_r^e + \frac{(1+\mu_2 k)\alpha_v\cdot r}{k+2} \tag{22}$$

By substituting Equations (11) and (22) into the fourth expression in Equation (8) of interface displacement continuity, the expression of P_1 is obtained.

3.2.3. Determination of Elastoplastic State of Frozen Wall

The radial and circumferential stress of the frozen wall are obtained by substituting P_1 into Equation (21). The maximum elastic external load occurs at the inner diameter of the frozen wall. Let $r = r_1$ and substitute the stress into strength Equation (7) for judgment: if $\sigma^e_{\theta(r=r_1)} < M\sigma^e_{r(r=r_1)} + N$, the frozen wall is in the elastic state shown in Figure 4a; otherwise, it is in the elastic–plastic state shown in Figure 4b.

3.3. Mechanical Calculation Model of Frozen Wall

The mechanical model of the frozen wall in the elastic–plastic state is illustrated in Figure 4b. The model can be divided into the plastic zone ($r \in [r_1, r_\rho]$), elastic zone ($r \in [r_\rho, r_2]$), and unfrozen zone ($r \in [r_2, r_\infty)$), where $r = r_\rho$ is the interface between the plastic zone of the frozen wall and the elastic zone, and $r = r_2$ is the interface between the elastic zone of the frozen wall and the unfrozen soil. In this case, the stress displacement boundary conditions are as follows:

$$\begin{cases} \sigma^p_r = 0 & (r = r_1) \\ \sigma^p_r = P_\rho & (r = r_\rho) \\ \sigma^e_r = P_\rho & (r = r_\rho) \\ \sigma^e_r = P_1 & (r = r_2) \\ \sigma^s_r = P_0 & (r = r_\infty) \\ U^e_r = U^s_r & (r = r_2) \\ U^\rho_r = U^e_r & (r = r_\rho) \end{cases}. \tag{23}$$

3.3.1. Plastic Zone of the Frozen Wall

The stress balance equation in the plastic zone of the frozen wall is expressed as follows:

$$\frac{d\sigma^p_r}{dr} + \frac{\sigma^p_r - \sigma^p_\theta}{r} = 0. \tag{24}$$

By substituting Equation (7) into Equation (24), the following formula can be obtained:

$$\frac{d\sigma^p_r}{dr} + \frac{(1-M)\sigma^p_r}{r} - \frac{Bc(r)}{r} = 0. \tag{25}$$

By solving the first-order constant coefficient differential Equation (25), the general solution of radial stress in the plastic zone of the frozen wall can be expressed as follows:

$$\sigma^p_r = B_1 l r^2 + B_2 m r + B_3 n + C_1 \cdot r^{M-1}, \tag{26}$$

where $B_1 = \frac{B}{3-M}$, $B_2 = \frac{B}{2-M}$, and $B_3 = \frac{B}{1-M}$.

According to the stress boundary conditions expressed in Equation (23), Equation (26) can be re-expressed as follows:

$$C_1 = (-B_1 l r_1^2 - B_2 m r_1 - B_3 n) \cdot r_1^{1-M}. \tag{27}$$

Therefore, the radial stress in the plastic zone of the frozen wall is expressed as

$$\sigma^p_r = B_1 l r^2 + B_2 m r + B_3 n - (B_1 l r_1^2 + B_2 m r_1 + B_3 n) \cdot \left(\frac{r}{r_1}\right)^{M-1}. \tag{28}$$

According to the strength criterion of frozen soil expressed in Equation (7), the circumferential stress of the plastic zone can be obtained:

$$\sigma_\theta^p = M\sigma_r^p + Bc(r) \quad r \in [r_1, r_\rho]. \tag{29}$$

The volume of the frozen wall is incompressible when it is in the plastic state, and the average strain is 0 [20–25]:

$$\varepsilon_m = \frac{\varepsilon_r + \varepsilon_\theta + \varepsilon_z}{3} = 0. \tag{30}$$

In the axisymmetric plane strain problem, Equation (30) can be simplified as

$$\varepsilon_r + \varepsilon_\theta = 0. \tag{31}$$

By substituting the geometric Equation (13) into Equation (31), the following formula is obtained:

$$\frac{du_r}{dr} + \frac{u_r}{r} = 0. \tag{32}$$

By solving the first-order homogeneous differential Equation (32) with variable coefficients, the general displacement solution of the plastic zone is obtained:

$$u_r = \frac{C_2}{r}. \tag{33}$$

According to the stress boundary conditions expressed in Equation (23), the following expression is obtained:

$$C_2 = \frac{r_\rho^2(1-\mu_2^2)((M - \frac{\mu_2}{1-\mu_2})P_\rho + B \cdot c(r_\rho))}{ar_\rho^2 + br_\rho + c} + (\alpha_\theta + \mu_2\alpha_r)r_\rho^2. \tag{34}$$

By substituting Equation (34) into Equation (33), the analytical solution of the plastic location shift can be obtained:

$$U^\rho = \frac{r_\rho^2(1-\mu_2^2)((M - \frac{\mu_2}{1-\mu_2})P_\rho + B \cdot c(r_\rho))}{r(ar_\rho^2 + br_\rho + c)} + \frac{(\alpha_\theta + \mu_2\alpha_r)r_\rho^2}{r}. \tag{35}$$

3.3.2. Elastic Region of the Frozen Wall

By substituting $\sigma^e_{r(r=r_\rho)} = P_\rho$ and $\sigma^e_{r(r=r_2)} = P_1$ in Equation (23) into Equation (18) and then into Equation (15), the analytical solution of stress under the elastoplastic state is obtained:

$$\begin{cases} \sigma_r^e = \dfrac{A_0H_2(A_5 - H_3) + (P_\rho - P_1 - A_0H_1)(A_6 - H_4)}{H_2} \\ \sigma_\theta^e = \dfrac{A_0H_2(A_8 - H_3) + (P_\rho - P_1 - A_0H_1)(A_7 - H_4)}{H_2} \end{cases}, \; r \in [r_\rho, r_2], \tag{36}$$

where $H_1 = a\left(r_\rho^2 - r_2^2\right) + 2b(r_\rho - r_2) + 2c\ln\frac{r_\rho}{r_2}$; $H_2 = a\ln\frac{r_\rho}{r_2} + b\left(\frac{1}{r_2} - \frac{1}{r_\rho}\right) + \frac{c}{2}\left(\frac{1}{r_2^2} - \frac{1}{r_\rho^2}\right)$; $H_3 = ar_2^2 + 2br_2 + 2c\ln r_2 - c$; $H_4 = a\ln r_2 - b\frac{1}{r_2} - \frac{c}{2}\frac{1}{r_2^2}$; $A_5 = ar^2 + 2br + 2c\ln r - c$; $A_6 = a\ln r - \frac{b}{r} - \frac{c}{2}\frac{1}{r^2}$; $A_7 = a\ln r + \frac{c}{2}\frac{1}{r^2} + a$; and $A_8 = 3ar^2 + 4br + 2c\ln r + c$.

By substituting Equation (36) into geometric Equation (13) and physical Equation (14), the displacement solution of the elastic region is obtained:

$$U^e = \frac{(1-\mu_2)\cdot r}{E(r)}\left(\sigma_\theta^e - \frac{\mu_2}{1-\mu_2}\cdot\sigma_r^e\right) + \frac{(1+\mu_2 k)\alpha_v}{k+2}\cdot r. \tag{37}$$

According to the above formula, when $r_\rho = r_1$ and $r_\rho = r_2$, $P_{1-\max}$ is the elastic ultimate load and plastic ultimate load, respectively.

3.3.3. Unfrozen Zone

In the elastic–plastic state of the frozen wall, the expressions of stress and displacement of the unfrozen soil are as follows [12,13]:

$$\sigma_r^s = \left(1 - \frac{r_2^2}{r^2}\right) P_0 + \frac{r_2^2}{r^2} P_1, \tag{38}$$

$$\sigma_\theta^s = \left(1 + \frac{r_2^2}{r^2}\right) P_0 - \frac{r_2^2}{r^2} P_1, \tag{39}$$

$$U^s = \frac{(1+\mu_3)(P_0 - P_1) r_2^2}{E_3 r}, \tag{40}$$

where E_3 and μ_3 are the elastic modulus and Poisson's ratio of unfrozen soil, respectively.

3.3.4. Radius of the Plastic Zone of the Frozen Wall

By combining Equations (23), (25), (28), (37) and (40), the following calculation formulas for P_1 and P_ρ are obtained:

$$P_\rho = B_1 l r_\rho^2 + B_2 m r_\rho + B_3 n - (B_1 l r_1^2 + B_2 m r_1 + B_3 n)\left(\frac{r_\rho}{r_1}\right)^{M-1}. \tag{41}$$

At the elastic–plastic junction, the stress in the elastic zone of the frozen wall meets the strength criterion of frozen soil:

$$\sigma_{r(r_\rho)}^e = M \sigma_{\theta(r_\rho)}^e + N_{(r_\rho)}. \tag{42}$$

By combining Equations (23), (36) and (42), the implicit equation of the radius of the plastic zone is obtained:

$$P_1 = \frac{P_0 H_2 (1+\mu_3) r_2^2 + (\alpha_\theta + \mu_2 \alpha_r) H_2 E_3 r_2^2}{(1+\mu_3)(1-\mu_2)(2H_2 r_2^2 - a r_2^2 - b r_2 - c)} - \frac{(P_\rho - A_0 H_1 + 2A_0 H_2 r_2^2)(a r_2^2 + b r_2 + c) H_2 r_2^2}{H_2 (2H_2 r_2^2 - a r_2^2 - b r_2 - c) r_2^2}, \tag{43}$$

$$\frac{(1-M) H_2 r_\rho^2 - a r_\rho^2 - b r_\rho - c}{H_2 r_\rho^2} P_\rho - \frac{(2A_0 H_2 r_\rho^2 - P_2 - A_0 H_1)(a r_\rho^2 + b r_\rho + c)}{H_2 r_\rho^2} = B(l r_\rho^2 + m r_\rho + n). \tag{44}$$

4. Mechanical Model of Frozen Wall

The inner and outer radii of the frozen wall of the new wind shaft considered in this study were 4 m and 10 m, respectively. The temperature at the freezing front was −3 °C. The thermal and physical parameters of the frozen soil are presented in Table 2. The coefficient of frost heave k was obtained by testing. Referring to the existing research results [11–15], k was set as 2.

Table 2. Thermophysical parameters of the frozen soil.

Elastic Modulus/MPa	Cohesive Force/MPa	Angle of Internal Friction	Poisson Ratio
−11.3T + 51.7	−0.26T + 1.17	10	0.35

The main external load of the frozen wall comes from formation pressure. Therefore, with the increase of the depth, the external load keeps increasing, and the stress state of the frozen wall changes accordingly. The stress distribution law of the frozen wall obtained by calculations at different depths is illustrated in Figure 5. According to the calculation

results, the external load acting on the shaft wall increased continuously with an increase in depth; thus, the radial stress and circumferential stress on the section of the frozen wall also increased. As the non-uniform characteristics of frozen wall were considered in the derivation of the calculation formula, the calculated circumferential stress approximately mimicked a parabolic variation. The maximum circumferential stress appeared near r = 1.5.

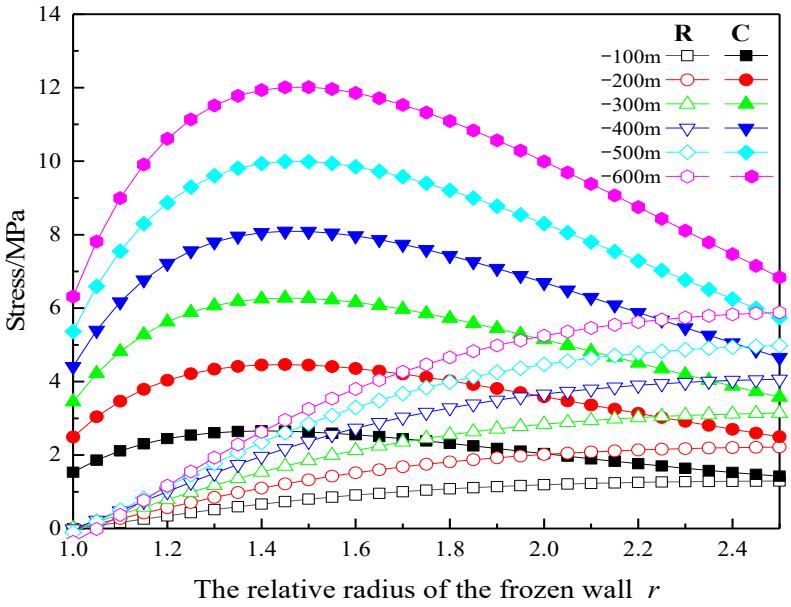


Figure 5. Stress distribution of the frozen wall at different depths. R represents the radial stress while C represents the circumferential stress.

In the process of the increase of the external load, the stress state of the frozen wall will go through three stages, namely, the elastic stage, the elastic–plastic stage, and the plastic stage. When the external load is small, the whole frozen wall is in the elastic state. When the external load increases to a certain critical value, the frozen wall enters the elastic–plastic state. The critical load from the elastic state into the plastic state is called the elastic limit load. When the frozen wall is in the elastic–plastic state, the frozen wall is divided into the plastic zone and the elastic zone from the inner edge to the outer edge. When the external load of the frozen wall increases further, the plastic zone expands gradually. When the whole frozen wall enters the plastic state, the corresponding external load is the plastic ultimate load. The stress state plays an important role in determining the stability of the frozen wall. The stress distribution of the frozen wall varies greatly under different stress states. Figure 6 illustrates the stress distribution of the frozen wall in the elastic limit state (p = 5.90 MPa), elastic–plastic state (p = 11.14 MPa), and plastic state (p = 16.39 MPa) according to the Mohr–Coulomb strength criterion. By comparison, the radial stress of the frozen wall increased with the increasing relative radius under different stress states, but the change law of circumferential stress was different. In the elastic limit state, elastoplastic state, and plastic limit state, the maximum circumferential stress of the frozen wall appeared at r = 1.5, the elastoplastic junction, and r = 2.0, respectively.

There are various yield criteria applicable to frozen soil. Currently, the commonly used ones are Mohr–Coulomb strength criteria, Druker–Prager strength criteria, Tresca strength criteria, and Twin shear unified failure criterion. Scholars usually choose one of these criteria as the basis for the calculation of mechanical properties of frozen wall [11–23]. In order to compare the difference of calculation results based on different criteria, the mechanical characteristics of frozen wall were calculated and analyzed with different yield criteria based on the same engineering condition in this study. Using different strength criteria, we calculated the elastic and plastic ultimate bearing capacity of the frozen wall at different average temperatures, as shown in Figures 7 and 8. The calculation results

show that the bearing capacity of the frozen wall increased with a decrease in the average temperature. The calculation results of the frozen wall bearing capacity varied with criteria. The calculation results based on the Mohr–Coulomb criterion were close to those based on the Druker–Prager criterion, and the calculation results based on the twin shear strength criterion were greater than those based on other criteria. When the average temperature of the frozen wall was −12 °C, the elastic ultimate bearing capacity calculated according to the twin shear strength criterion, Tresca strength criterion, Mohr–Coulomb strength criterion, and Druker–Prager strength criterion was 5.35, 4.78, 4.06, and 4.03 MPa, respectively; the plastic bearing capacity was 15.79, 13.64, 11.11, and 11.03 MPa, respectively. When the average temperature of the frozen wall was −20 °C, the ultimate elastic bearing capacity calculated according to the twin shear strength criterion, Tresca strength criterion, Mohr–Coulomb strength criterion, and Druker–Prager strength criterion was 7.77, 6.94, 5.90, and 5.86 MPa, respectively; the plastic ultimate bearing capacity was 23.28, 20.14, 16.39, and 16.27 MPa, respectively.

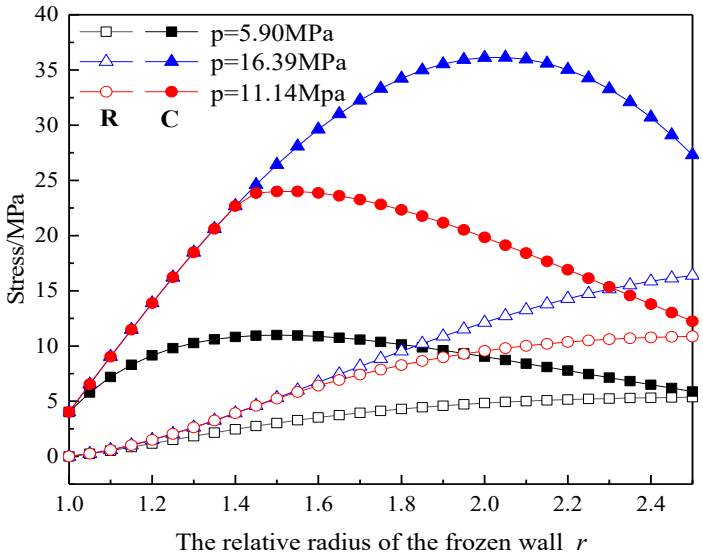


Figure 6. Stress distribution of the frozen wall under different stress states. R represents the radial stress while C represents the circumferential stress.

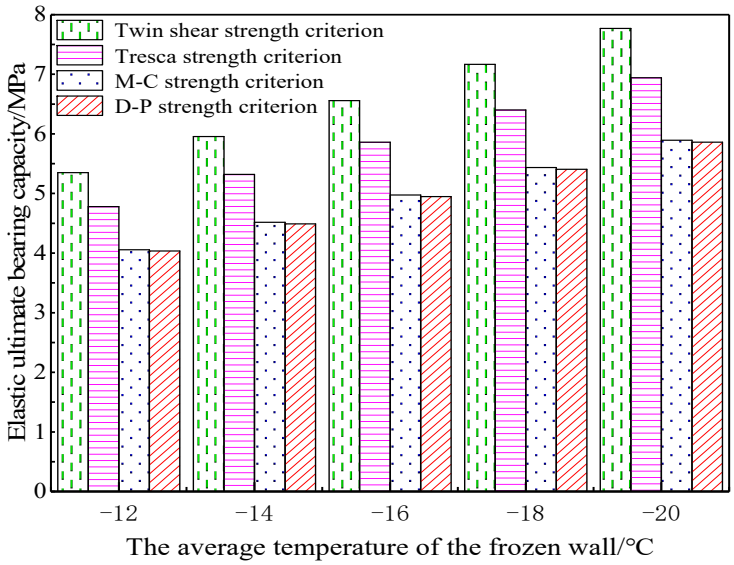


Figure 7. Calculation results of the elastic ultimate bearing capacity.

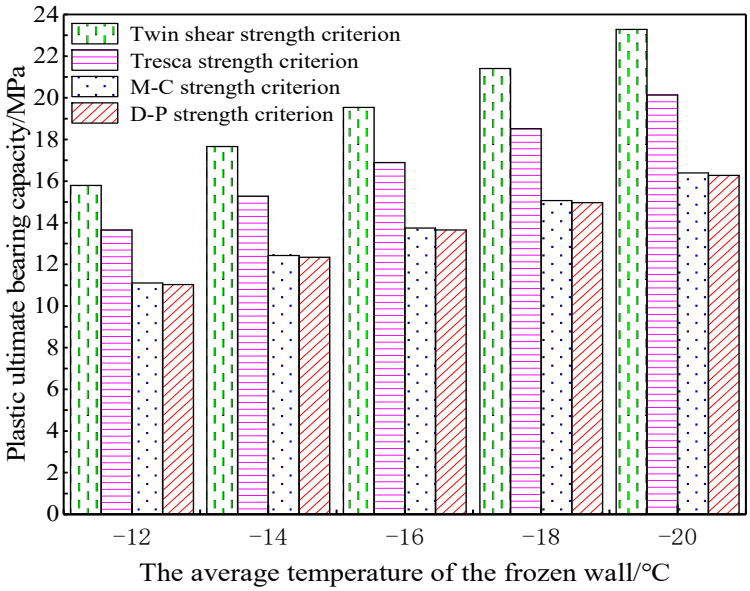


Figure 8. Calculation results of the plastic ultimate bearing capacity.

In the elastic limit and plastic limit states, the stress calculation results of the frozen wall based on different yield criteria are illustrated in Figures 9 and 10. A comparison shows that under the two stress states, the distribution law of the radial stress of the frozen wall was similar and increased with the increasing relative radius; the distribution law of the circumferential stress was significantly different. Although the circumferential stress of the frozen wall changed in an approximately parabolic shape under both conditions, the maximum value of the circumferential stress appeared at r = 1.5 in the elastic limit state and at r = 2.0 in the plastic limit state.

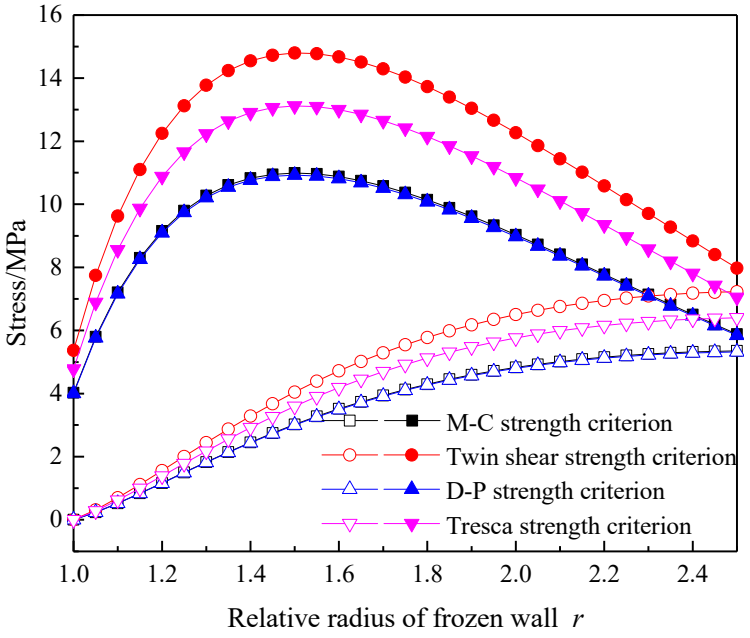


Figure 9. Stress distribution of the frozen wall in the elastic limit state.

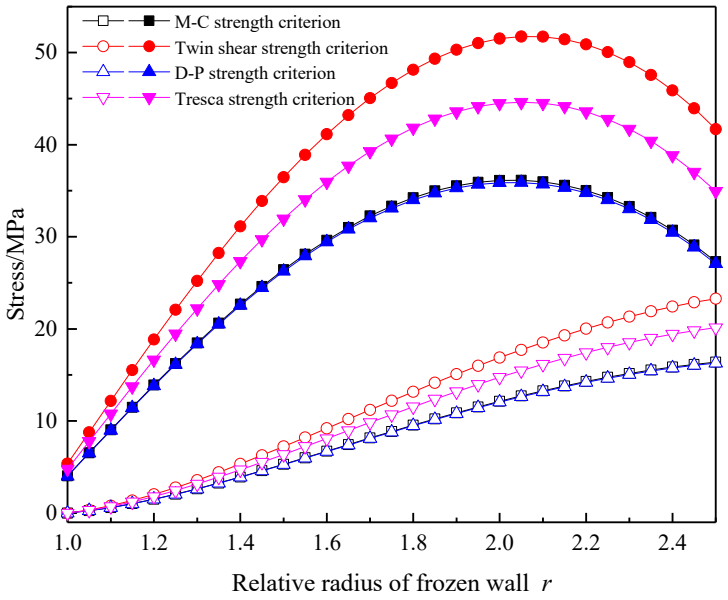


Figure 10. Stress distribution of the frozen wall in the plastic limit state.

The relationship between the bearing capacity of the frozen wall and the radius of the plastic zone was determined through calculations, and the results are illustrated in Figure 11. The results show that when the frozen wall entered the plastic state, its bearing capacity increased with the increase in the radius of the plastic zone, but the growth rate decreased gradually. Therefore, the larger the radius of the plastic zone was, the greater the damage risk of the frozen wall. The calculation results varied according to yield criteria, and the calculation results based on the Mohr–Coulomb and Druker–Prager criteria were mostly similar; the calculation results based on the twin shear strength criterion was the largest.

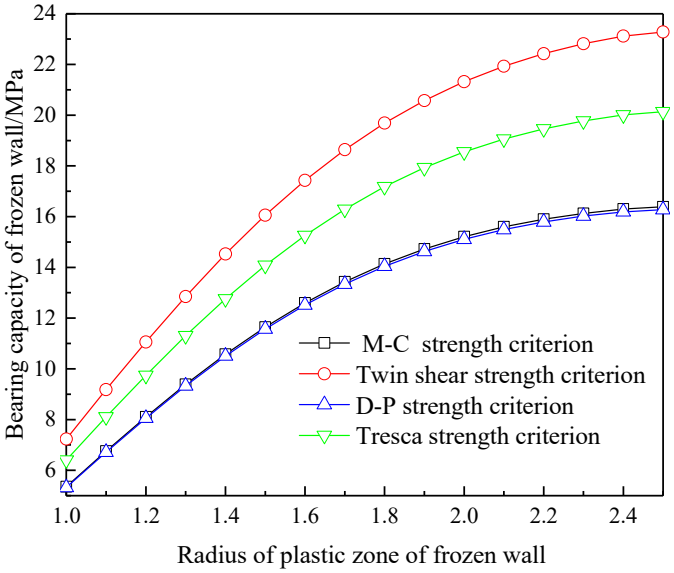


Figure 11. Relationship between plastic zone radius and bearing capacity of frozen wall.

The most common manifestation of frost heave in the freezing of a shaft is the displacement of the inner and outer edges of the frozen wall. The displacements of the inner and outer edges of the frozen wall in this study were calculated at different depths, as shown in Figure 12. As the depth increased, the external load of the frozen wall increased, and the displacement of the outer and inner edges of the frozen wall also increased. The lower the average temperature was, the greater the bearing capacity of the frozen wall; thus, the

lower the average temperature was, the smaller the displacement of the frozen wall. The displacement of the outer edge of the frozen wall was always greater than that of the inner edge, which changed with temperature significantly more than that of the outer edge.

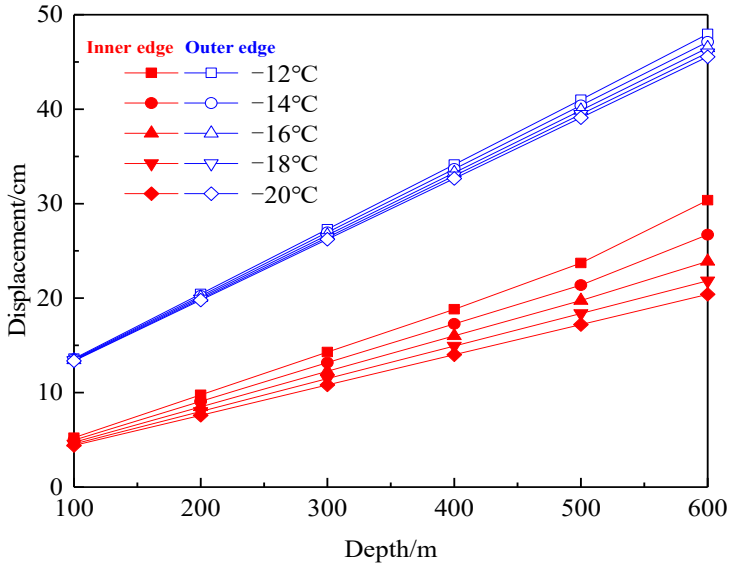


Figure 12. Variation of displacement of the inner edge and outer edge of the frozen wall.

When the average temperature was −20 °C, the relationship between the inner edge displacement and the radius of the plastic zone calculated based on different strength criteria was obtained, as illustrated in Figure 13. The results show that the displacement of increased rapidly with the increase in the radius of the plastic zone. When the relative radius *r* of the plastic zone reached 1.8, the calculated displacement results based on the twin shear strength criterion, Tresca strength criterion, Mohr–Coulomb strength criterion, and Druker–Prager strength criterion were 134.5, 118.2, 98.6, and 98.0 cm, respectively, which all exceed the allowable displacement range of the frozen wall. When a part of the frozen wall entered the plastic state, the displacement of the whole frozen wall increased considerably. Therefore, the bearing capacity of the frozen wall should be improved by increasing the thickness of the frozen wall or reducing the average temperature of the frozen wall, which would minimize the chances of the frozen wall entering the plastic state.

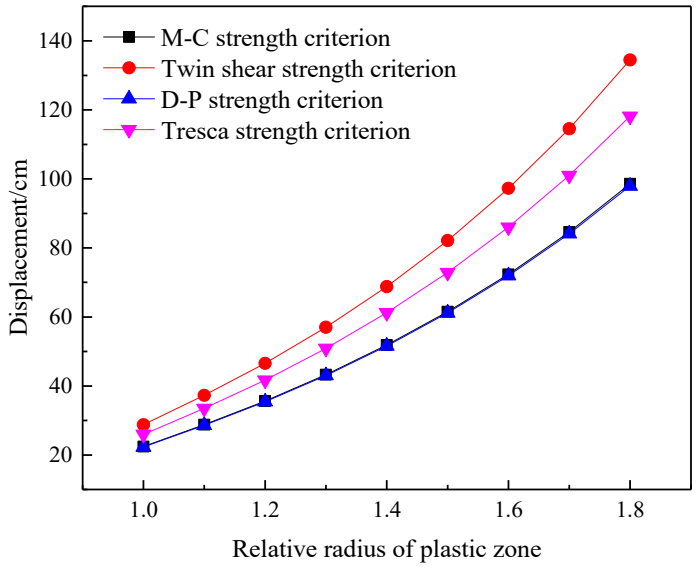


Figure 13. Variation of frozen wall displacement with plastic zone radius.

The results obtained using the heterogeneous frozen wall displacement formula derived in this paper, considering frost heave characteristics, were compared with the results of the frozen wall displacement formula without considering frost heave (converted from Ref. [20]). Figures 14 and 15 illustrate the comparison. The results show that the displacement mainly comprised two parts: the displacement generated by the frozen wall in the elastic or elastic–plastic state under the action of external load, and the displacement caused by soil frost heave. When the frost heave property was not considered, the calculated displacement of the frozen wall was smaller. Further analysis showed that the displacement of the inner and outer edges of the frozen wall due to frost heave remained unchanged when the buried depth was 100–300 m. In the depth range of 500–600 m, the frozen wall entered the elastoplastic state, and the displacement of the inner edge of the frozen wall caused by frost heave increased with the increase in the plastic zone. Meanwhile, the displacement of the outer edge caused by frost heave decreased with the increase in the plastic zone. A comparison of the displacements of the inner and outer edges showed that the total displacement of the outer edge of the frozen wall was greater than that of the inner edge at the same burial depth. Moreover, the displacement of frost heave on the outer edge was greater than that on the inner edge.

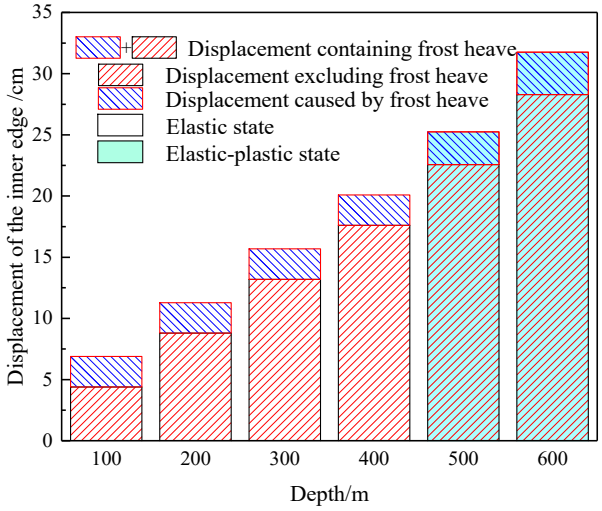


Figure 14. Comparison of the calculation results of the frozen wall inner edge displacement of the before and after frost heaving.

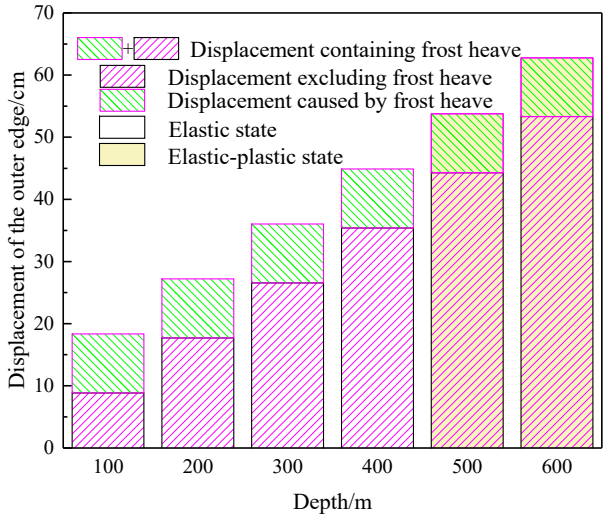


Figure 15. Comparison of the calculation results of the frozen wall outer edge displacement before and after considering frost heaving.

5. Conclusions

1. When the non-uniform characteristics were considered, the radial stress varied linearly with the relative radius r, and the circumferential stress of the frozen wall varied approximately in a parabolic shape. In this case, under the elastic limit state, the maximum value of the circumferential stress of the frozen wall appeared at $r = 1.5$. In the elastoplastic state, the maximum circumferential stress appeared at the elastoplastic junction. In the plastic limit state, the maximum circumferential stress appeared at $r = 2.0$;
2. The displacement of the outer and inner edges of the frozen wall increased with the increase in formation depth; the lower the average temperature of the frozen wall was, the smaller the displacement value. The displacement of the outer edge of the frozen wall was always greater than that of the inner edge, but the influence of temperature on the inner edge was greater than that of the outer edge;
3. When the frozen wall was in the elastic state, the displacement caused by frost heave was constant. However, when the frozen wall entered the elastic–plastic state, the displacement of the inner edge of the frozen wall caused by frost heave increased with the increase in the plastic zone, and the displacement of the outer edge of the frozen wall caused by frost heave decreased with the increase in the plastic zone;
4. When the frozen wall entered the plastic state, its bearing capacity increased with the increase in the radius of the plastic zone, but the growth rate decreased gradually. When a part of the frozen wall entered the plastic state, the displacement of the whole frozen wall increased considerably. Therefore, to improve the stability of the frozen wall, its bearing capacity should be enhanced by increasing its thickness or decreasing its average temperature, which would prevent the plastic state of the frozen wall.

Author Contributions: Conceptualization, B.W.; methodology, S.L.; software, Y.C.; validation, C.R., S.Y.; formal analysis, B.W.; investigation, B.W.; resources, B.W.; data curation, S.L.; writing—original draft preparation, B.W.; writing—review and editing, B.W.; visualization, S.L.; supervision, Y.C.; project administration, B.W.; funding acquisition, B.W. All authors have read and agreed to the published version of the manuscript.

Funding: This work was support by the Natural Science Foundation of Anhui Province (Grant No. 2108085QE251), China Postdoctoral Science Foundation (Grant No. 2021M703621), Anhui Postdoctoral Science Foundation (Grant No. 2022B635), Open Fund grants projects of Engineering Research Center of Underground Mine Construction of Ministry of Education (Grant No. JYBGCZX2022103), Key Project of Natural Science Research in Universities of Anhui Province (KJ2021A0425), Natural Science Foundation of Anhui University of Science and technology (xjzd2020-18), Talent Introduction Project of Anhui University of Science and Technology (13200403), Major Science and Technology Special Project of Anhui Province (202003c08020007), College student innovation and entrepreneurship program (S202210361048).

Institutional Review Board Statement: Not applicable.

Informed Consent Statement: Informed consent was obtained from all subjects involved in the study.

Data Availability Statement: The data used to support the findings of this study are available from the corresponding author upon request.

Conflicts of Interest: The authors declare that they have no known competing financial interests or personal relationships that could have appeared to influence the work reported in this paper.

References

1. Liu, Y.; Li, K.Q.; Li, D.Q.; Tang, X.S.; Gu, S.X. Coupled thermal–hydraulic modeling of artificial ground freezing with uncertainties in pipe inclination and thermal conductivity. *Acta Geotech.* **2022**, *17*, 257–274. [CrossRef]
2. Wang, B.; Rong, C.; Cheng, H.; Cai, H. Experimental investigation on heat transfer law of multiple freezing pipes in permeable stratum with high seepage velocity. *Int. J. Heat Mass Transf.* **2022**, *182*, 121868. [CrossRef]
3. Wang, B.; Rong, C.; Cheng, H. Analytical Solution of Steady-state Temperature Field of Asymmetric Frozen Wall Induced by Directional Seepage. *Adv. Eng. Sci.* **2022**, *54*, 76–87. (In Chinese)

4. Rong, C.; Wang, B.; Cheng, H.; Dong, Y.; Yang, F. Laboratory model test study on formation mechanisms of artificial frozen walls in permeable strata with high seepage velocity. *Chin. J. Rock Mech. Eng.* **2022**, *41*, 596–613. (In Chinese)
5. Yang, Z. Deformation Behaviour and Design Method of Icewall in Deep Soil Based on Co-bearing of Icewall and Stratum. Ph.D. Thesis, China University of Mining and Technology, Beijing, China, 2019. (In Chinese).
6. Ghiasi, V.; Omar, H.; Huat, B.B.K.; Muniandi, R.; Zainuddin, B. Risk management overview of tunnels using numerical modeling. *J. Eng. Des. Technol.* **2011**, *9*, 110–124. [CrossRef]
7. Ghiasi, V.; Koushki, M. Numerical and artificial neural network analyses of ground surface settlement of tunnel in saturated soil. *SN Appl. Sci.* **2020**, *2*, 939. [CrossRef]
8. Ghiasi, V.; Omar, H. Analysis of shotcrete lining of underground tunnels. *Pertanika J. Sci. Technol.* **2011**, *19*, 249–257.
9. Cao, G.; Cheng, H.; Rong, C. Theoretical solution to freezing pressure in Jurassic strata based on Kelvin damage model. *J. Min. Saf. Eng.* **2021**, *38*, 972–978. (In Chinese)
10. He, P.; Ma, W.; Mu, Y.; Dong, J.; Huang, Y. Elastic foundation beam model for frost heave damage of trapezoidal canal lining considering frost heave force and adfreeze force. *J. Cent. South Univ. Sci. Technol.* **2021**, *52*, 4148–4157. (In Chinese)
11. Zhang, C.; Gao, B.; Zhou, W.; Li, H. Plastic solutions of a cold region tunnel under freeze-thawcycles and non-uniform frost heave. *Chin. J. Theor. Appl. Mech.* **2022**, *54*, 252–262. (In Chinese)
12. Zhang, C.; Gao, B.; Li, T.; Shan, Y. An elastic-plastic solution for frost heaving force of cold region tunnels considering transversely isotropic frost heave and displacement release. *Rock Soil Mech.* **2021**, *42*, 2967–2976. (In Chinese)
13. Zhang, C.; Gao, B.; Shan, Y.; Li, Z. Unified plastic solution for stress and displacement of tunnels in cold regions considering transversely isotropic frost heave. *Chin. J. Geotech. Eng.* **2020**, *42*, 1825–1831. (In Chinese)
14. Xia, C.; Lv, Z.; Li, Q.; Huang, J.; Bai, X. Transversely isotropic frost heave of saturated rock under unidirectional freezing condition and induced frost heaving force in cold region tunnels. *Cold Reg. Sci. Technol.* **2018**, *152*, 48–58. [CrossRef]
15. Lv, Z.; Xia, C.; Wang, Y.; Luo, J. Analytical elasto-plastic solution of frost heaving force in cold region tunnels considering transversely isotropic frost heave of surrounding rock. *Cold Reg. Sci. Technol.* **2019**, *163*, 87–97. [CrossRef]
16. Feng, Q.; Jiang, B.; Zhang, Q.; Wang, L. Analytical elasto-plastic solution for stress and deformation of surrounding rock in cold region tunnels. *Cold Reg. Sci. Technol.* **2014**, *108*, 59–68. [CrossRef]
17. Liu, W.; Feng, Q.; Fu, S.; Wang, C. Elasto-plastic solution for cold-regional tunnels considering the compound effect of non-uniform frost heave, supporting strength and supporting time. *Tunn. Undergr. Space Technol.* **2018**, *82*, 293–302. [CrossRef]
18. Zhang, Y.; Xie, Y.; Li, Y.; Lai, J. A frost heave model based on space-time distribution of temperature field in cold region tunnels. *Rock Soil Mech.* **2018**, *39*, 1625–1632. (In Chinese)
19. Jiang, W.; Jiang, H.; Ma, Q.; Li, Y.; Li, Z. Unified elasto-plastic solution for cold regions tunnel considering damage and non-uniform frost heave. *J. South China Univ. Technol. Nat. Sci. Ed.* **2022**, *50*, 69–79+100. (In Chinese)
20. Hu, X.; Shu, C.; She, S. Elastic-plastic analytical solution for functionally graded material frozen soil wall with parabolic property under uniform load. *J. China Coal Soc.* **2012**, *37*, 379–384. (In Chinese)
21. Hu, X.; Shu, C. Stress field analysis of functionally graded material frozen soil wall in double-row-pipe shaft freezing. *Eng. Mech.* **2014**, *31*, 145–153. (In Chinese)
22. Wang, B.; Rong, C.; Cheng, H. Elastic and Plastic Analysis of Heterogeneous Frozen Soil Wall of Triple-row Piped Freezing. *J. Yangtze River Sci. Res. Inst.* **2019**, *36*, 104–111. (In Chinese)
23. Wang, B.; Rong, C.; Cheng, H.; Cai, H. Analysis of mechanical properties of heterogeneous frozen wall induced by directional seepage. *J. Glaciol. Geocryol.* **2022**, *44*, 1011–1020. (In Chinese)
24. Yang, W.; Yang, Z.; Bo, D. Elastic-plastic design theory of frozen soil wall based on interaction between frozen wall and surrounding rock. *Chin. J. Geotech.* **2013**, *35*, 175–180. (In Chinese)
25. Wang, B.; Rong, C.; Cheng, H. Stress analysis of heterogeneous frozen wall considering interaction with surrounding soil. *J. China Coal Soc.* **2017**, *42*, 354–361. (In Chinese)

Disclaimer/Publisher's Note: The statements, opinions and data contained in all publications are solely those of the individual author(s) and contributor(s) and not of MDPI and/or the editor(s). MDPI and/or the editor(s) disclaim responsibility for any injury to people or property resulting from any ideas, methods, instructions or products referred to in the content.